

Electrochemical Reduction of N₂O with a Molecular Copper Catalyst

Jorge L. Martinez, Joseph E. Schneider, Sophie W. Anferov, and John S. Anderson*



Cite This: ACS Catal. 2023, 13, 12673–12680



Read Online

ACCESS |

Metrics & More

Article Recommendations

Supporting Information

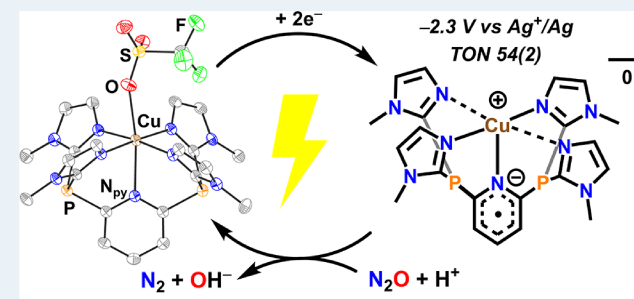
ABSTRACT: Deoxygenation of nitrous oxide (N₂O) has significant environmental implications, as it is not only a potent greenhouse gas but is also the main substance responsible for the depletion of ozone in the stratosphere. This has spurred significant interest in molecular complexes that mediate N₂O deoxygenation. Natural N₂O reduction occurs via a Cu cofactor, but there is a notable dearth of synthetic molecular Cu catalysts for this process. In this work, we report a selective molecular Cu catalyst for the electrochemical reduction of N₂O to N₂ using H₂O as the proton source. Cyclic voltammograms show that increasing the H₂O concentration facilitates the deoxygenation of N₂O, and control experiments with a Zn(II) analogue verify an essential role for Cu. Theory and spectroscopy support metal–ligand cooperative catalysis between Cu(I) and a reduced tetraimidazolyl-substituted radical pyridine ligand (MeIm₄P₂Py = 2,6-(bis(bis-2-N-methylimidazolyl)phosphino)pyridine), which can be observed by Electron Paramagnetic Resonance (EPR) spectroscopy. Comparison with biological processes suggests a common theme of supporting electron transfer moieties in enabling Cu-mediated N₂O reduction.

KEYWORDS: N₂O reduction, N₂O reductase, homogeneous catalysis, electrocatalysis, redox-active ligand, denitrification

INTRODUCTION

Nitrous oxide (N₂O) is the leading ozone-depleting substance of this century, rivaling many hydrochlorofluorocarbons (HCFCs).¹ N₂O is also a potent greenhouse gas with a long atmospheric lifetime (>100 years) and is 10× and 300× more warming by mass than CH₄ and CO₂, respectively.^{2,3} Thus, decomposition of N₂O is important in order to mitigate its effect on climate. Of possible decomposition routes, the reduction of N₂O to N₂ and H₂O is attractive due to the formation of benign byproducts. However, deoxygenation remains difficult, as even thermal decomposition is limited by a large kinetic barrier ($\Delta G^\ddagger = 59$ kcal/mol in the gas phase) despite being thermodynamically favorable ($\Delta G = -81$ kcal/mol).^{4,5} The poor σ -donating and π -accepting properties of N₂O lead to sluggish binding kinetics with transition metals, which also limits their chemistry with N₂O.^{6,7} This problem is reflected by the small number of N₂O adducts that have been characterized structurally and/or spectroscopically.^{8–14}

Approximately two-thirds of anthropogenic N₂O is derived from excess Haber–Bosch nitrogen (i.e., fertilizers) through incomplete bacterial denitrification.^{15–17} Some denitrification bacteria contain the gene for nitrous oxide reductase (N₂OR), the only known enzyme capable of reducing N₂O as its natural substrate to N₂ and H₂O through a 2e[−]/2H⁺ process.¹⁸ N₂OR is a Cu-based metalloenzyme consisting of two Cu clusters: a binuclear copper site responsible for electron transfer, Cu_A, and a tetranuclear μ_4 -sulfido bridged cluster, Cu_Z^{*}, which is the active site for N₂O binding and reduction.^{19,20} Computational



Electrochemical N₂O Reduction with Cu

and spectroscopic studies suggest that N₂OR overcomes the high kinetic barrier for N–O cleavage by binding N₂O in a μ -1,3 fashion assisted by H-bonding from the secondary coordination sphere (Figure 1a),^{21,22} although there is some controversy over this mechanistic proposal.^{23–25}

Despite the importance of Cu in biological N₂O reduction, and elegant synthetic work aimed at isolating structurally and chemically faithful active site mimics,^{26–33} molecular Cu catalysts for the reduction of N₂O to N₂ and H₂O/OH[−] are not known. Nevertheless, stoichiometric reactions with di- and trinuclear Cu species suggest that tetranuclear copper sites are not required for N₂O reduction.³⁴ Favorable binding of N₂O to Cu(I) suggests that even monometallic systems should also be considered.^{8,35}

Despite the lack of synthetic Cu-based N₂O reduction catalysts, homogeneous thermal hydrogenation of N₂O to N₂ and H₂O has been reported with second and third row transition metal catalysts, namely, Ru, Rh, Pt, and Ir.^{36–39} Mixtures of N₂O and H₂ are potentially explosive,^{40,41} and this has also spurred interest in electrochemical reduction of N₂O as an effective route.⁴² Still, while several exciting examples of

Received: June 12, 2023

Revised: August 29, 2023

Published: September 14, 2023



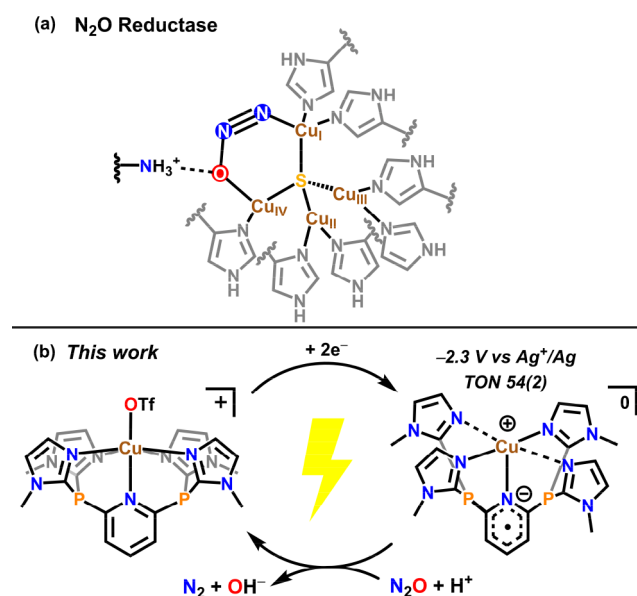


Figure 1. (a) Proposed binding of N_2O in the $4\text{Cu}^{\text{I}}:\text{S}$ active site of N_2O reductase and (b) electrochemical N_2O reduction catalysis in this work.

molecular N_2O electrocatalysts have recently been reported, no examples of Cu-based catalysts have been shown despite Cu's biological relevance.^{43–48}

These considerations motivated us to investigate the synthesis of a new N_2O reduction electrocatalyst based on Cu. Herein we report the first molecular Cu complex capable of electrocatalytically reducing N_2O in MeCN using water as a proton source. Electrochemical studies show that this catalyst operates with excellent selectivity for N_2O reduction vs hydrogen evolution. Mechanistic analysis suggests that ligand redox noninnocence plays an important role, as verified by both computations and spectroscopy, and this observation may suggest a more general need for additional electron storing ligands/metals in molecular N_2O reduction catalysis.

RESULTS AND DISCUSSION

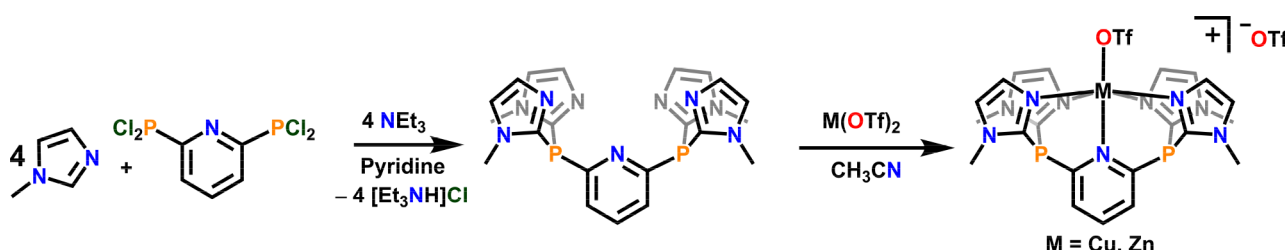
Catalyst Synthesis and Characterization. It has previously been shown that some organic radicals are competent outer-sphere redox catalysts for the electrochemical reduction of N_2O in MeCN,⁴⁷ and we were particularly inspired by catalysis using 4-cyanopyridine.⁴⁹ We were interested in investigating a pyridine donor that could be used as an effective electron shuttle for Cu-catalyzed N_2O reduction (Figure 1b). Since demetalation of $\text{Cu}(\text{I})$ is a common deactivation pathway in Cu_z^* synthetic models, we rationalized that polydentate chelates with strong N donors

could minimize the loss of this labile metal.^{30,33} We previously reported a Co(II) compound supported by a tip(Me) ligand ($\text{tip}(\text{Me}) = 2,6\text{-bis}(\text{bis}-2\text{-N-methylimidazolyl})\text{-hydroxymethyl}$) for electrocatalytic water oxidation featuring strongly donating imidazole arms such as PY5Me₂ (PY5Me₂ = 2,6-bis(1,1-bis(2-pyridyl)ethyl)-pyridine).^{51–54} We aimed to further redesign this ligand to remove the acidic hydroxyl groups and to increase synthetic ease by replacing the carbon bridgeheads with P atoms. This new tetraimidazolyl-substituted pyridine ligand, MeIm₄P₂Py (MeIm₄P₂Py = 2,6-(bis(bis-2-N-methylimidazolyl)-phosphino)pyridine, **1**), was synthesized by adapting a previously described one-pot reaction between a dichlorophosphine and an *N*-alkyl imidazole (Scheme 1).⁵⁵ Addition of 2,6-(Cl₂P)Py to a mixture of *N*-methylimidazole and NEt₃ in pyridine at room temperature affords **1** in a good yield after workup (60%).

Metalation was carried out by the addition of Cu(OTf)₂ to a slurry of sparingly soluble **1** in MeCN, affording $[(\text{MeIm}_4\text{P}_2\text{Py})\text{Cu}(\text{OTf})][\text{OTf}]$ (**1-Cu**) as an air-stable blue powder in excellent yield after recrystallization (82%). Crystals suitable for single-crystal X-ray diffraction (SXRD) were obtained by the slow vapor diffusion of Et₂O into MeCN at room temperature. The solid-state structure of **1-Cu** (Figure 2) reveals the pentadentate coordination of **1** to Cu with one inner sphere triflate ion. This six-coordinate species contains notably long axial bonds (Cu–O = 2.487(2) Å, Cu–N_{Py} = 2.432(2) Å) consistent with a Jahn–Teller distortion in tetragonally elongated Cu(II). Imidazole bond distances ($\langle \text{Cu}–\text{N}_{\text{Im}} \rangle$ = 2.022(2) Å) are slightly shorter than the nonelongated copper-pyridine distances in the analogous six-coordinate $[(\text{PY5Me}_2)\text{Cu}(\text{MeCN})]^{2+}$ complex ($\langle \text{Cu}–\text{N}_{\text{Py}} \rangle$ = 2.044(4) Å).⁵⁶ The metal center lies only 0.085 Å from the plane defined by the four imidazole N atoms. This is in contrast to our previously reported $[\text{Co}(\text{tip}(\text{Me}))(\text{CH}_3\text{CN})][\text{OTf}]_2$ complex, which shows the metal “puckered” 0.213 Å away from the N_{Im} plane.⁵⁰ This main structural difference between **1** and tip(Me) can be attributed to the larger size of phosphorus compared to carbon.

The frozen solution EPR spectrum of **1-Cu** (15 K) is consistent with a Cu(II) $S = 1/2$ assignment (Figure S39). Paramagnetically shifted resonances in the ¹H NMR spectrum of **1-Cu** also support this d⁹ assignment (Figure S7), and Evan's method shows an expected solution moment of 1.71(4) μ_{B} . The number of resonances in the ¹H NMR spectrum is also in agreement with the solid-state C_{2v} symmetry. A sharp singlet in the ¹⁹F{¹H} NMR spectrum that is slightly shifted from free triflate suggests weakly ion paired triflate counteranions in CD₃CN solution. Rapid ligand exchange between outer sphere

Scheme 1. Complex Synthesis



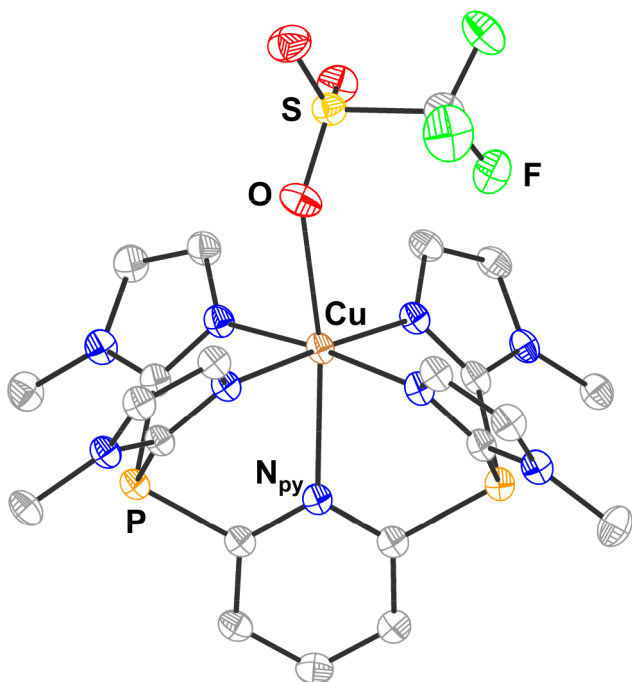


Figure 2. Solid-state structure of **1-Cu**. Ellipsoids are shown at 50% probability, and hydrogen atoms have been omitted for clarity. C is shown in gray, N is shown in blue, O is shown in red, F is shown in green, P is shown in orange, S is shown in yellow, and Cu is shown in brown. Selected bond lengths (Å) and angles (°) are as follows: Cu–N_{Im} 2.048(2), 2.013(2), 2.028(2), and 1.997(2); Co–N_{Py} 2.432(2); Co–O 2.487(2); O–Cu–N_{Py} 170.81(7); N5–Cu–N7 87.35(8); and N7–Cu–N3 92.67(8).

triflate and MeCN is possible, if not likely, in solution. Additionally, a very broad resonance can be observed in the $^{31}\text{P}\{\text{H}\}$ NMR spectrum of **1-Cu** ($\delta = -48$ ppm) in concentrated samples, corresponding to the bridging P atoms of the ligand with a chemical shift similar to that of **1** ($\delta = -45.2$ ppm).

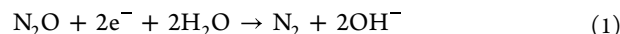
Electrochemical Characterization. Cyclic voltammetry (CV) of **1-Cu** in MeCN revealed three reduction processes. The first quasi-reversible wave at -0.8 V vs Fc^+/Fc corresponds to a metal-centered Cu(II)/Cu(I) redox couple with a large peak-to-peak separation ($\Delta E_p = 200$ mV at 100 mV s $^{-1}$). A similarly large ΔE_p was observed in the previously reported PY5Me₂ analog.⁵⁶ Scan rate studies show an increase in ΔE_p of **1-Cu** with increasing scan rates, which indicates a changing coordination environment upon reduction from Cu(II) to Cu(I).⁵⁷ The two remaining irreversible cathodic processes appear at $E_{p,c} = -2.15$ V and $E_{p,c} = -2.75$ V vs Fc^+/Fc and are tentatively assigned as Cu(I)L/Cu(I)L $^{\bullet-}$ and Cu(I)L $^{\bullet}/\text{Cu(I)L}^{2-}$ ligand-based reductions, respectively (L = 1; Figure S15). These assignments are supported by the CV of **1** in MeCN, which shows that the substituted pyridine ligand can be reduced by 1 e^- in the absence of a metal (Figure S23).

To confirm the presence of ligand-based reductions in the CV of **1-Cu**, the control complex $[(\text{MeIm}_4\text{P}_2\text{Py})\text{ZnOTf}][\text{OTf}]$ (**1-Zn**) was synthesized following a similar procedure as its Cu(II) analog. An octahedral ligand field environment similar to that of **1-Cu** is observed in the SXRD structure of **1-Zn** (Figure S43). The average Zn–N_{Im} (2.118(1) Å) bond is slightly shorter than the average Zn–N_{Py} distance (2.153(4) Å) in its PY5Me₂ analog, consistent with the stronger donor properties of the imidazole donors.⁵⁸ Most notably, **1-Zn** also

contains an unusually long axial Zn–N_{Py} bond (2.380(2) Å), which is again likely enforced by the longer bridging P–C bonds in ligand **1**.⁵⁹

The CV of **1-Zn** in MeCN shows three cathodic processes (Figure S21), with the first irreversible wave assigned as the Zn(II)L $^{2+}/\text{Zn(II)L}^{\bullet+}$ redox couple ($E_{p,c} = -1.83$ V). The remaining two, presumably ligand-based, irreversible reductions are at very negative potentials ($E_{p,c} = -2.54$ V and $E_{p,c} = -2.73$ V). Notably, the reduction of **1-Zn** is milder than that of the analogous $[\text{Zn}(\text{PY5Me}_2)(\text{MeCN})]^{2+}$ complex, suggesting that the phosphine groups in **1** are more electron-withdrawing toward the apical pyridine ring.⁶⁰ The ligand-based reduction potential in **1-Zn** is significantly shifted from those of **1-Cu** ($E_{p,c} = -2.15$ V) and the free ligand **1** ($E_{1/2} = -2.68$ V). These differences in potential can be attributed to the differences in charge between the three species. Regardless of these differences, all of these CV studies support the viability of a ligand-based reduction in this system.

Electrocatalysis. In dry solvent and electrolyte, the first two reduction potentials in the CV of **1-Cu** under an atmosphere of N_2O do not shift, suggesting that there is no binding of N_2O prior to the reduction of the complex (Figure 3A). A catalytic current is observed upon the addition of water, and a slight anodic shift is observed with increasing equivalents (Figure 3B). The stoichiometry of this reaction is described in eq 1.



Reduction of N_2O occurs after the ligand is reduced, as can be seen by the inflection in the catalytic wave after the Cu(I)L/Cu(I)L $^{\bullet-}$ redox couple (Figure 3A, blue trace). The slight anodic shift in the inflection point with increasing water concentration could suggest that water facilitates binding to Cu(I) and promotes N–O bond cleavage. Evidence of significant water coordination to Cu was not found, as the reduction potentials of **1-Cu** remained unchanged with high concentrations of water in the absence of N_2O (Figure S19). Similar electrochemical behavior is observed when the $\text{N}^+\text{Bu}_4\text{OTf}$ supporting electrolyte is used instead of $\text{N}^+\text{Bu}_4\text{PF}_6^-$, which excludes competitive OTf $^-$ binding in solution (Figure S18). The CV of **1-Zn** in the presence of N_2O shows that it is not a competent N_2O reduction electrocatalyst, and we note that the reduction potential of ligand **1** is beyond the onset for the direct reduction of N_2O with glassy carbon (see the SI for details). Both observations highlight the importance of Cu for electrocatalysis with this framework.

Controlled potential electrolysis (CPE) in the presence of 1 atm N_2O and 100 mM H_2O using a reticulated vitreous carbon (RVC) working electrode was performed at -2.3 V for 1 h to investigate the product selectivity of **1-Cu**. A linear increase of charge passed over time is seen up until ~ 9 C is passed, after which charge consumption plateaus, indicating loss of activity (Figure 3C). This hypothesis is also supported by the slow drop in current over the course of electrolysis, which suggests catalyst degradation, as has been observed in related systems.⁴⁷ We note that only a low amount of background activity by the RVC electrode was observed in the absence of **1-Cu** under identical conditions. Headspace analysis using TCD GC found N_2 to be the only gaseous product, with no detectable H_2 . Additionally, only a small amount of H_2 is produced in the absence of N_2O under identical conditions (Figures S34 and S36), indicating that **1-Cu** is not competent for proton reduction under these conditions. An average turnover number

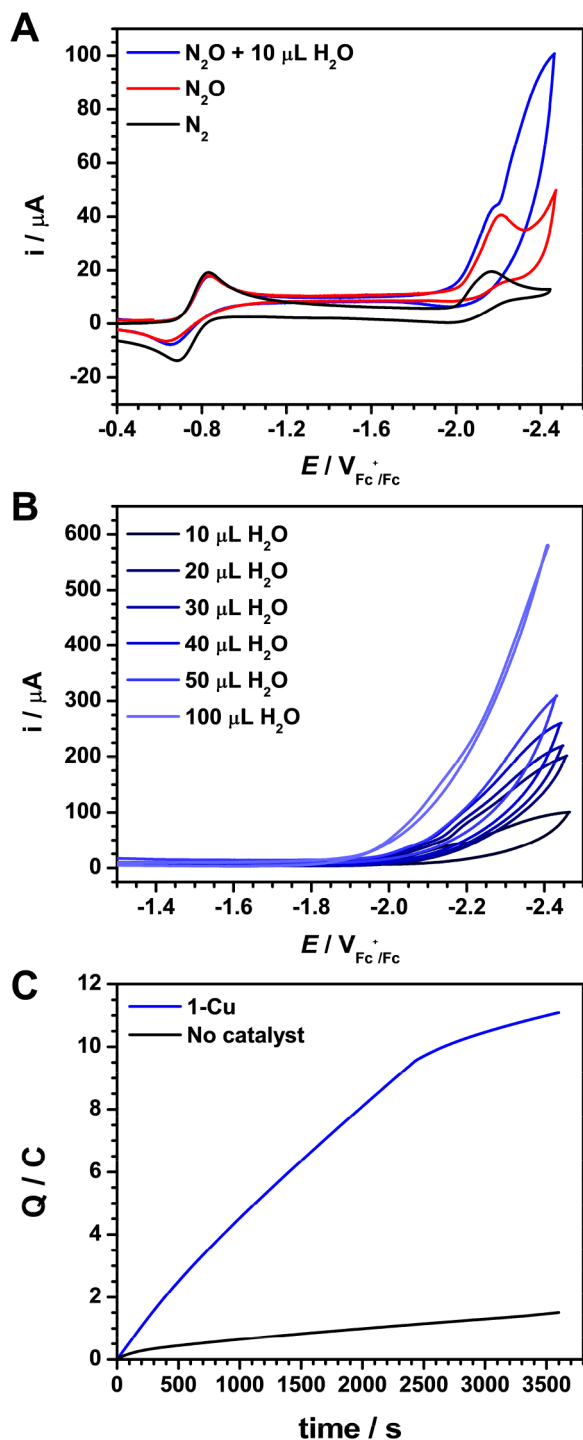


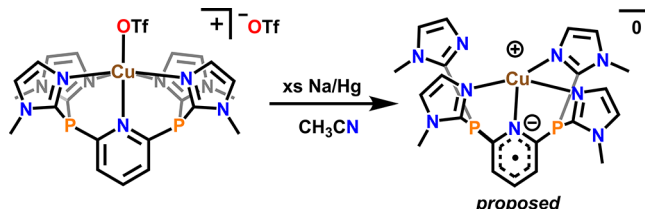
Figure 3. Cyclic voltammograms (scan rate 100 mV s⁻¹) recorded using a 3 mm diameter glassy carbon working electrode in MeCN and 0.1 M $\text{N}^{\text{t}}\text{Bu}_4\text{PF}_6$ supporting electrolyte for (a) 1-Cu under 1 atm N_2 (black), N_2O (red), and N_2O in the presence of 10 μL (0.1 M) of water (blue) and (b) 1-Cu under 1 atm of N_2O with increasing amounts of water: 10 (0.11 M), 20 (0.22 M), 30 (0.33 M), 40 (0.44 M), 50 (0.55 M), and 100 μL (1.11 M). (c) Controlled potential electrolysis at -2.3 V (vs Ag^+/Ag) of a MeCN solution of 0.1 M $\text{N}^{\text{t}}\text{Bu}_4\text{PF}_6$ supporting electrolyte with H_2O (100 mM) under 1 atm N_2O using a RVC working electrode. Charge passed as a function of time in the presence of catalyst (1-Cu, 1 mM) is shown in blue, and that in the absence of catalyst is shown in black.

(TON) of 54(2) was determined over the course of 1 h with a Faradaic efficiency of 83(8)% for N_2 . This nonquantitative Faradaic yield likely arises from decreasing activity over time due to catalyst degradation, presumably from competing reactions with water or the OH^- product⁶¹ as well as the limited stability of the reduced species. Further evidence of this is supported by the CV of 1-Cu, which shows the instability of the reduced species in the presence of water at slower scan rates (Figure S19). Finally, CV of the solution after CPE using a glassy carbon plate (Figure S27) shows no electrochemical features, suggesting that the decomposition product(s) is electrochemically inactive. Indeed, a significant amount of free ligand, which is electrochemically inactive at the applied potential, was identified by ¹H and ³¹P{¹H} NMR spectroscopy after CPE (Figures S28 and S29).

Mechanistic Investigations. The electrochemical activity of 1-Cu prompted us to perform chemical and theoretical investigations of possible mechanistic steps. We hypothesized that any N_2O reduction would necessarily proceed from an initially reduced congener of 1-Cu. We therefore investigated the reactivity of 1-Cu with the reducing agents. We initially tested catalytic chemical reduction of N_2O using 0.1% Na/Hg as a reducing agent under conditions similar to those used in CPE experiments (see the SI). Although there is significant activity from Na/Hg and H_2O in the absence of catalyst, the presence of 1 mol % 1-Cu more than doubles the amount of N_2 generated, with nearly all reducing agent consumed (Figure S33), supporting Cu-mediated catalysis. This observation also supports the use of Na/Hg as a surrogate for electrochemical reduction in mechanistic probes of 1-Cu.

We then attempted to obtain a more detailed characterization of the reduction products by chemically reducing 1-Cu with Na/Hg in MeCN (Scheme 2). *In situ* monitoring of this

Scheme 2. Reduction of 1-Cu by 2e⁻ using Excess Na/Hg



reduction by UV-visible spectroscopy shows the disappearance of the initial d-d transitions in the spectrum, followed by a slow growth of two bands at approximately 410 and 680 nm over the course of 1 h (Figure S38). We propose that these absorption bands are related to the catalytically relevant species, since the Cu(I) intermediate is expected to have no signal in the visible region, consistent with our observations.

To test this hypothesis, characterization of this putative odd-electron-reduced species was attempted using EPR spectroscopy. An EPR signal consistent with an $S = 1/2$ complex distinct from the EPR signal of the Cu(II) starting complex was observed in a MeCN frozen solution (33 K) (Figure 4A). The frozen-solution EPR spectrum of the reduction of 1-Zn (Figure S40) shows a similar but distinct signal that supports the viability of ligand-based radicals in this system. The signal from the reduction of 1-Cu can be simulated with $g = 2.010$, 2.013, and 2.012, $A(^{63}\text{Cu}) = 12$, 11, and 7 MHz, and $A(^{14}\text{N}) = 42$, 3, and 2 MHz, consistent with a primarily pyridine centered radical. We note this signal is qualitatively similar to a

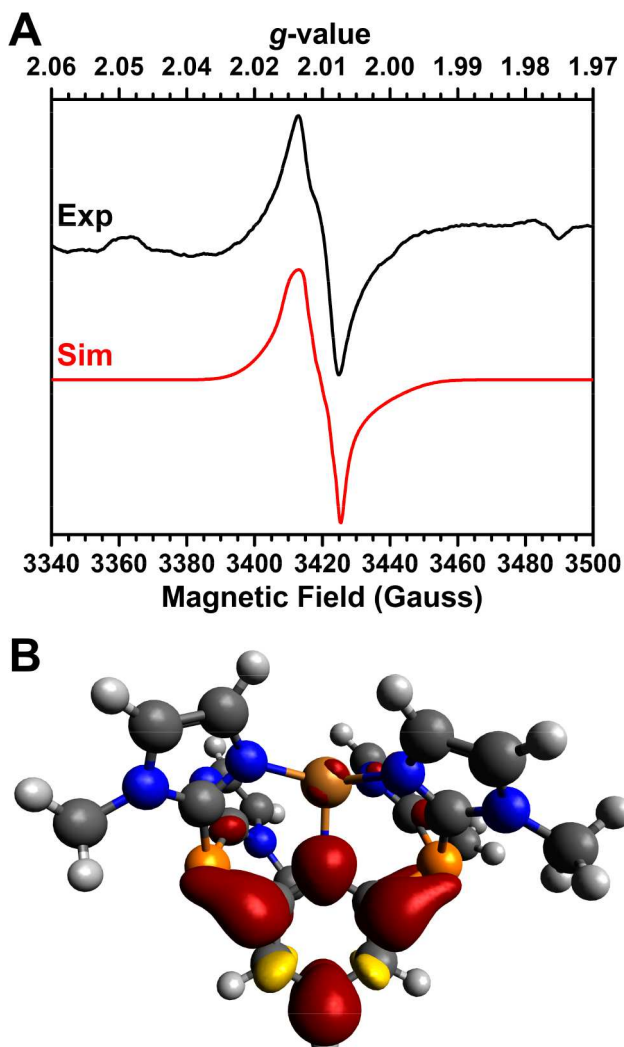


Figure 4. (A) EPR spectrum of the Na/Hg reduction of **1-Cu**. (B) Spin density plot of the $2e^-$ reduced model complex (isovalue of 0.002). EPR conditions are as follows: microwave frequency of 9.6304 GHz, microwave power of 0.2 mW, and modulation of 0.03 mT/100 kHz.

previously reported 2,6-disubstituted pyridine radical (broad single line, peak-to-peak 120 G).⁶²

We also performed DFT calculations on possible reduced complexes to gain insight into the catalytically relevant species (Figure S44). Geometry optimizations of a singly reduced Cu(I) intermediate predict a four-coordinate geometry with one ligand arm dissociated. This prediction is consistent with the structural changes inferred from the quasi-reversible redox couple in the CV of **1-Cu** at -0.8 V vs Fc⁺/Fc. Further reduction by an additional electron is ligand-based, as illustrated by the spin density, which is primarily on the pyridine donor with some delocalization onto the imidazole arms through the σ^* of the P–C bond (Figure 4B). We have performed calculations of the EPR parameters of this complex, which match the values obtained from simulation of the experimental spectrum well. Namely, both DFT and simulation support moderate hyperfine coupling to N and Cu (Table S1).

It is important to note that there are multiple thermodynamically accessible isomers for these reduced species that may contribute to catalyst degradation, as has been reported in a similar NS species for water reduction (see SI).⁶³ Thus, the

depicted geometry of this doubly reduced intermediate is only a model, and other coordination geometries and ligation environments (different solvates, for example) are possible if not likely. We hypothesize that this reduced species then rapidly reacts with N₂O and water to generate N₂ and OH[−], consistent with the catalytic onset that is observed just beyond the second reduction event in the CV of **1-Cu**. Indeed, CV with variable concentrations of **1-Cu** and H₂O suggests first-order behavior in both of these reagents, consistent with this hypothesis (Figure S20). Regardless of the exact reduced speciation of **1-Cu**, the spectroscopy and calculations support a vital role for ligand redox noninnocence as an electron storage/shuttling mechanism for catalysis. This echoes possible roles for the multi-Cu cluster in biological N₂O reduction and may point to a more fundamental requirement for additional redox cofactors in N₂O reduction catalysis by Cu.

CONCLUSION

We report the first example of a molecular Cu catalyst for N₂O reduction. This complex, **1-Cu**, enables electrocatalytic reduction of N₂O with water to afford N₂ with a high Faradaic efficiency. Catalytic reduction with a chemical reducing agent was also demonstrated with dilute Na/Hg. Electrochemical studies support the onset of catalysis after reduction of **1-Cu** twice, and a combination of spectroscopy and theory supports the importance of ligand-based reductions in forming reduced intermediates. While **1-Cu** is a highly unusual example of a Cu-based catalyst for N₂O reduction, we do note that previous molecular electrocatalysts with other transition metals show higher Faradaic efficiencies (>90%) and less decomposition.^{43–48} For instance, [Re(2,2'-bipyridine)(CO)₃Cl] boasts ~200 turnovers over the course of 2 h with no significant catalyst degradation, albeit with a comparatively precious metal.⁴⁸ The findings reported here provide an initial proof-of-concept validation for further efforts toward the design of new Cu-based molecular electrocatalysts for N₂O reduction. In addition to improved performance metrics and increasing the stability of the active catalyst, there remain interesting mechanistic questions surrounding both electron transfer principles and details about N₂O binding, reduction, and protonation events.

ASSOCIATED CONTENT

Supporting Information

The Supporting Information is available free of charge at <https://pubs.acs.org/doi/10.1021/acscatal.3c02658>.

Experimental procedures, NMR spectra, electrochemistry data, TCD GC spectra and calibration curves, UV-visible spectra, EPR spectra, SXRD data, and DFT calculations (PDF)

1-Cu (CIF)

1-Zn (CIF)

XYZ files of three-coordinate Cu(I) with and without a reduced ligand, four-coordinate Cu(I) with and without a reduced ligand, Cu(II) with and without OTf, and OTf (ZIP)

Accession Codes

CCDC 2266810 and 2266811 contain the supplementary crystallographic data for this paper. These data can be obtained free of charge via www.ccdc.cam.ac.uk/data_request/cif, or by emailing data_request@ccdc.cam.ac.uk, or by contacting The

Cambridge Crystallographic Data Centre, 12 Union Road, Cambridge CB2 1EZ, UK; fax: + 44 1223 336033.

AUTHOR INFORMATION

Corresponding Author

John S. Anderson – Department of Chemistry, University of Chicago, Chicago, Illinois 60637, United States;
ORCID.org/0000-0002-0730-3018; Email: jsanderson@uchicago.edu

Authors

Jorge L. Martinez – Department of Chemistry, University of Chicago, Chicago, Illinois 60637, United States
Joseph E. Schneider – Department of Chemistry, University of Chicago, Chicago, Illinois 60637, United States
Sophie W. Anferov – Department of Chemistry, University of Chicago, Chicago, Illinois 60637, United States;
ORCID.org/0000-0003-3972-5845

Complete contact information is available at:
<https://pubs.acs.org/10.1021/acscatal.3c02658>

Author Contributions

J.L.M. designed and performed experimental work and wrote the manuscript. J.E.S. collected EPR data, performed computational investigations, and assisted with the manuscript. S.W.A. collected and refined X-ray data for the solid-state structure investigations and assisted with the manuscript. J.S.A. supervised the project and assisted in writing and editing the manuscript.

Notes

The authors declare no competing financial interest.

ACKNOWLEDGMENTS

This research was supported by the National Institutes of Health (R35 GM133470). J.E.S. thanks the Department of Defense for a National Defense Science and Engineering Graduate Fellowship (00003765), and J.S.A. thanks the Sloan Foundation for a Research Fellowship (FG-2019-11497) and the Dreyfus Foundation for a Teacher-Scholar award (TC-21-064). Single crystal X-ray diffraction data reported here were collected at ChemMatCARS Sector 15, which is supported by the NSF under Grant NSF/CHE-1834750. This research used resources of the APS, a U.S. DOE Office of Science User Facility operated for the DOE Office of Science by Argonne National Laboratory under contract no. DE-AC02-06CH11357. We would like to thank Dr. Yu-Sheng Chen for assistance with SXRD acquisition at 15-ID-B,C,D. TCD GC data were collected in the University of Chicago Mass Spectrometry facility and was supported by SF instrumentation Grant CHE-1048528. The authors are grateful for the support of the University of Chicago Research Computing Center for assistance with the calculations carried out in this work. J.L.M. would like to thank Krista M. Kulesa for inspiring the research topic and insightful discussions in electrochemistry. J.L.M. would also like to thank the Wuttig group for providing helpful insights to the group for CPE experimental setup.

REFERENCES

- (1) Ravishankara, A. R.; Daniel, J. S.; Portmann, R. W. Nitrous Oxide (N_2O): The Dominant Ozone-Depleting Substance Emitted in the 21st Century. *Science* **2009**, *326* (5949), 123–125.
- (2) Rodhe, H. A Comparison of the Contribution of Various Gases to the Greenhouse Effect. *Science* **1990**, *248* (4960), 1217–1219.
- (3) Montzka, S. A.; Dlugokencky, E. J.; Butler, J. H. Non- CO_2 greenhouse gases and climate change. *Nature* **2011**, *476* (7358), 43–50.
- (4) Johnston, H. S. Interpretation of the Data on the Thermal Decomposition of Nitrous Oxide. *J. Chem. Phys.* **1951**, *19* (6), 663–667.
- (5) Lee, D.-H.; Mondal, B.; Karlin, K. D. Nitrogen Monoxide and Nitrous Oxide Binding and Reduction. In *Activation of Small Molecules* **2006**, 43–79.
- (6) Tolman, W. B. Binding and Activation of N_2O at Transition-Metal Centers: Recent Mechanistic Insights. *Angew. Chem., Int. Ed.* **2010**, *49* (6), 1018–1024.
- (7) Severin, K. Synthetic chemistry with nitrous oxide. *Chem. Soc. Rev.* **2015**, *44* (17), 6375–6386.
- (8) Zhuravlev, V.; Malinowski, P. J. A Stable Crystalline Copper(I)– N_2O Complex Stabilized as the Salt of a Weakly Coordinating Anion. *Angew. Chem., Int. Ed.* **2018**, *57* (36), 11697–11700.
- (9) Paulat, F.; Kuschel, T.; Näther, C.; Praneeth, V. K. K.; Sander, O.; Lehnert, N. Spectroscopic Properties and Electronic Structure of Pentammineruthenium(II) Dinitrogen Oxide and Corresponding Nitrosyl Complexes: Binding Mode of N_2O and Reactivity. *Inorg. Chem.* **2004**, *43* (22), 6979–6994.
- (10) Armor, J. N.; Taube, H. Formation and reactions of $[(NH_3)_5RuN_2O^{2+}]$. *J. Am. Chem. Soc.* **1969**, *91* (24), 6874–6876.
- (11) Piro, N. A.; Licherman, M. F.; Harman, W. H.; Chang, C. J. A Structurally Characterized Nitrous Oxide Complex of Vanadium. *J. Am. Chem. Soc.* **2011**, *133* (7), 2108–2111.
- (12) Gyton, M. R.; Leforestier, B.; Chaplin, A. B. Rhodium(I) Pincer Complexes of Nitrous Oxide. *Angew. Chem., Int. Ed.* **2019**, *58* (43), 15295–15298.
- (13) Mokhtarzadeh, C. C.; Chan, C.; Moore, C. E.; Rheingold, A. L.; Figueroa, J. S. Side-On Coordination of Nitrous Oxide to a Mononuclear Cobalt Center. *J. Am. Chem. Soc.* **2019**, *141* (38), 15003–15007.
- (14) Puerta Lombardi, B. M.; Gendy, C.; Gelfand, B. S.; Bernard, G. M.; Wasylisen, R. E.; Tuononen, H. M.; Roesler, R. Side-on Coordination in Isostructural Nitrous Oxide and Carbon Dioxide Complexes of Nickel. *Angew. Chem., Int. Ed.* **2021**, *60* (13), 7077–7081.
- (15) Richardson, D.; Felgate, H.; Watmough, N.; Thomson, A.; Baggs, E. Mitigating release of the potent greenhouse gas N_2O from the nitrogen cycle – could enzymic regulation hold the key? *Trends Biotechnol.* **2009**, *27* (7), 388–397.
- (16) Tavares, P.; Pereira, A. S.; Moura, J. J. G.; Moura, I. Metalloenzymes of the denitrification pathway. *J. Inorg. Biochem.* **2006**, *100* (12), 2087–2100.
- (17) Thomson, A. J.; Giannopoulos, G.; Pretty, J.; Baggs, E. M.; Richardson, D. J. Biological sources and sinks of nitrous oxide and strategies to mitigate emissions. *J. Philos. Trans. R. Soc.* **2012**, *367* (1593), 1157–1168.
- (18) Pauleta, S. R.; Dell'Acqua, S.; Moura, I. Nitrous oxide reductase. *Coord. Chem. Rev.* **2013**, *257* (2), 332–349.
- (19) Brown, K.; Tegoni, M.; Prudêncio, M.; Pereira, A. S.; Besson, S.; Moura, J. J.; Moura, I.; Cambillau, C. A novel type of catalytic copper cluster in nitrous oxide reductase. *Nat. Struct. Biol.* **2000**, *7* (3), 191–195.
- (20) Chen, P.; Gorelsky, S. I.; Ghosh, S.; Solomon, E. I. N_2O Reduction by the μ_4 -Sulfide-Bridged Tetranuclear Cu_2 Cluster Active Site. *Angew. Chem., Int. Ed.* **2004**, *43* (32), 4132–4140.
- (21) Gorelsky, S. I.; Ghosh, S.; Solomon, E. I. Mechanism of N_2O Reduction by the μ_4 -S Tetranuclear CuZ Cluster of Nitrous Oxide Reductase. *J. Am. Chem. Soc.* **2006**, *128* (1), 278–290.
- (22) Johnston, E. M.; Carreira, C.; Dell'Acqua, S.; Dey, S. G.; Pauleta, S. R.; Moura, I.; Solomon, E. I. Spectroscopic Definition of the Cu_2 ⁺ Intermediate in Turnover of Nitrous Oxide Reductase and Molecular Insight into the Catalytic Mechanism. *J. Am. Chem. Soc.* **2017**, *139* (12), 4462–4476.

(23) Pomowski, A.; Zumft, W. G.; Kroneck, P. M. H.; Einsle, O. N_2O binding at a [4Cu:2S] copper–sulphur cluster in nitrous oxide reductase. *Nature* **2011**, *477* (7363), 234–237.

(24) Wüst, A.; Schneider, L.; Pomowski, A.; Zumft, W. G.; Kroneck, P. M. H.; Einsle, O. Nature's way of handling a greenhouse gas: the copper-sulfur cluster of purple nitrous oxide reductase. *Biol. Chem.* **2012**, *393* (10), 1067–1077.

(25) Johnston, E. M.; Dell'Acqua, S.; Ramos, S.; Pauleta, S. R.; Moura, I.; Solomon, E. I. Determination of the Active Form of the Tetrานuclear Copper Sulfur Cluster in Nitrous Oxide Reductase. *J. Am. Chem. Soc.* **2014**, *136* (2), 614–617.

(26) Johnson, B. J.; Lindeman, S. V.; Mankad, N. P. Assembly, Structure, and Reactivity of Cu_4S and Cu_3S Models for the Nitrous Oxide Reductase Active Site, Cu_2^* . *Inorg. Chem.* **2014**, *53* (19), 10611–10619.

(27) Johnson, B. J.; Antholine, W. E.; Lindeman, S. V.; Mankad, N. P. A Cu_4S model for the nitrous oxide reductase active sites supported only by nitrogen ligands. *Chem. Commun.* **2015**, *51* (59), 11860–11863.

(28) Johnson, B. J.; Antholine, W. E.; Lindeman, S. V.; Graham, M. J.; Mankad, N. P. A One-Hole Cu_4S Cluster with N_2O Reductase Activity: A Structural and Functional Model for Cu_2^* . *J. Am. Chem. Soc.* **2016**, *138* (40), 13107–13110.

(29) Hartmann, N. J.; Wu, G.; Hayton, T. W. Synthesis and reactivity of a nickel(II) thioperoxide complex: demonstration of sulfide-mediated N_2O reduction. *Chem. Sci.* **2018**, *9* (31), 6580–6588.

(30) Hsu, C.-W.; Rathnayaka, S. C.; Islam, S. M.; MacMillan, S. N.; Mankad, N. P. N_2O Reductase Activity of a $[\text{Cu}_4\text{S}]$ Cluster in the 4Cu¹ Redox State Modulated by Hydrogen Bond Donors and Proton Relays in the Secondary Coordination Sphere. *Angew. Chem., Int. Ed.* **2020**, *59* (2), 627–631.

(31) Rathnayaka, S. C.; Hsu, C.-W.; Johnson, B. J.; Iniguez, S. J.; Mankad, N. P. Impact of Electronic and Steric Changes of Ligands on the Assembly, Stability, and Redox Activity of $\text{Cu}_4(\mu_4\text{S})$ Model Compounds of the Cu_2^* Active Site of Nitrous Oxide Reductase (N_2OR). *Inorg. Chem.* **2020**, *59* (9), 6496–6507.

(32) Rathnayaka, S. C.; Islam, S. M.; DiMucci, I. M.; MacMillan, S. N.; Lancaster, K. M.; Mankad, N. P. Probing the electronic and mechanistic roles of the μ_4 -sulfur atom in a synthetic Cu_2^* model system. *Chem. Sci.* **2020**, *11* (13), 3441–3447.

(33) Rathnayaka, S. C.; Mankad, N. P. Coordination chemistry of the Cu_2^* site in nitrous oxide reductase and its synthetic mimics. *Coord. Chem. Rev.* **2021**, *429*, 213718.

(34) Sinhababu, S.; Lakliang, Y.; Mankad, N. P. Recent advances in cooperative activation of CO_2 and N_2O by bimetallic coordination complexes or binuclear reaction pathways. *Dalton Trans.* **2022**, *51* (16), 6129–6147.

(35) Wang, G.; Jin, X.; Chen, M.; Zhou, M. Matrix isolation infrared spectroscopic and theoretical study of the copper (I) and silver (I)–nitrous oxide complexes. *Chem. Phys. Lett.* **2006**, *420* (1), 130–134.

(36) Zeng, R.; Feller, M.; Ben-David, Y.; Milstein, D. Hydrogenation and Hydrosilylation of Nitrous Oxide Homogeneously Catalyzed by a Metal Complex. *J. Am. Chem. Soc.* **2017**, *139* (16), 5720–5723.

(37) Jurt, P.; Abels, A. S.; Gamboa-Carballo, J. J.; Fernández, I.; Le Corre, G.; Aebl, M.; Baker, M. G.; Eiler, F.; Müller, F.; Wörle, M.; Verel, R.; Gauthier, S.; Trincado, M.; Gianetti, T. L.; Grützmacher, H. Reduction of Nitrogen Oxides by Hydrogen with Rhodium(I)–Platinum(II) Olefin Complexes as Catalysts. *Angew. Chem., Int. Ed.* **2021**, *60* (48), 25372–25380.

(38) Ortega-Lepe, I.; Sánchez, P.; Santos, L. L.; Lara, P.; Rendón, N.; López-Serrano, J.; Salazar-Pereira, V.; Alvarez, E.; Paneque, M.; Suárez, A. Catalytic Nitrous Oxide Reduction with H_2 Mediated by Pincer Ir Complexes. *Inorg. Chem.* **2022**, *61* (46), 18590–18600.

(39) Böksén, J.; Rodríguez-Lugo, R. E.; Nappen, S.; Trincado, M.; Grützmacher, H. Reduction of Nitrous Oxide by Light Alcohols Catalysed by a Low-Valent Ruthenium Diazadiene Complex. *Chem. Eur. J.* **2023**, *29* (20), e202203632.

(40) Wang, L.-Q.; Ma, H.-H.; Shen, Z.-W. Explosion characteristics of $\text{H}_2/\text{N}_2\text{O}$ and $\text{CH}_4/\text{N}_2\text{O}$ diluted with N_2 . *Fuel* **2020**, *260*, 116355.

(41) Wang, L.-Q.; Li, T.; Ma, H.-H. Explosion behaviors of hydrogen-nitrous oxide mixtures at reduced initial pressures. *Process Saf. Environ. Prot.* **2021**, *153*, 11–18.

(42) Niemann, V. A.; Benedek, P.; Guo, J.; Xu, Y.; Blair, S. J.; Corson, E. R.; Nielander, A. C.; Jaramillo, T. F.; Tarpeh, W. A. Co-designing Electrocatalytic Systems with Separations To Improve the Sustainability of Reactive Nitrogen Management. *ACS Catal.* **2023**, *13*, 6268–6279.

(43) Collman, J. P.; Marrocco, M.; Elliott, C. M.; L'Her, M. Electrocatalysis of nitrous oxide reduction: Comparison of several porphyrins and binary “face-to-face” porphyrins. *J. Electroanal. Chem. Interfacial Electrochem.* **1981**, *124* (1), 113–131.

(44) Taniguchi, I.; Shimpuku, T.; Yamashita, K.; Ohtaki, H. Electrocatalytic reduction of nitrous oxide to dinitrogen at a mercury electrode using nnn complexes of macrocyclic polyamines. *J. Chem. Soc. Chem. Commun.* **1990**, *13*, 915–917.

(45) Zhang, J.; Tse, Y.-H.; Lever, A. B. P.; Pietro, W. J. Electrochemical reduction of nitrous oxide (N_2O) catalysed by tetraaminophthalocyanatocobalt(II) adsorbed on a graphite electrode in aqueous solution. *J. Porphyrins Phthalocyanines* **1997**, *1* (4), 323–331.

(46) Tezuka, M.; Iwasaki, M. Cobalt Tetraphenylporphine Electrocatalyzed N_2O Reduction in DMF Solution. *Chem. Lett.* **1998**, *27* (10), 1017–1018.

(47) Deeba, R.; Chardon-Noblat, S.; Costentin, C. Homogeneous molecular catalysis of the electrochemical reduction of N_2O to N_2 : redox vs. chemical catalysis. *Chem. Sci.* **2021**, *12* (38), 12726–12732.

(48) Deeba, R.; Molton, F.; Chardon-Noblat, S.; Costentin, C. Effective Homogeneous Catalysis of Electrochemical Reduction of Nitrous Oxide to Dinitrogen at Rhenium Carbonyl Catalysts. *ACS Catal.* **2021**, *11* (10), 6099–6103.

(49) Deeba, R.; Chardon-Noblat, S.; Costentin, C. Molecular Catalysis of Electrochemical Reactions: Competition between Reduction of the Substrate and Deactivation of the Catalyst by a Cosubstrate Application to N_2O Reduction. *ChemElectroChem.* **2021**, *8* (19), 3740–3744.

(50) McMillion, N. D.; Wilson, A. W.; Goetz, M. K.; Chang, M.-C.; Lin, C.-C.; Feng, W.-J.; McCrory, C. C. L.; Anderson, J. S. Imidazole for Pyridine Substitution Leads to Enhanced Activity Under Milder Conditions in Cobalt Water Oxidation Electrocatalysis. *Inorg. Chem.* **2019**, *58* (2), 1391–1397.

(51) Carty, A. J.; Minchin, N. J.; Skelton, B. W.; White, A. H. Interaction of palladium(II) acetate with substituted pyridines, including a cyclometallation reaction and the structure of $[\text{Pd}\{meso-[(py)PhMeC]\}_2\text{C}_5\text{H}_3\text{N}\}(\text{O}_2\text{CMe})][\text{O}_2\text{CMe}] \cdot 3\text{H}_2\text{O}$. *J. Chem. Soc., Dalton Trans.* **1986**, *10*, 2205–2210.

(52) Bechlars, B.; D'Alessandro, D. M.; Jenkins, D. M.; Iavarone, A. T.; Glover, S. D.; Kubiak, C. P.; Long, J. R. High-spin ground states via electron delocalization in mixed-valence imidazolate-bridged divanadium complexes. *Nat. Chem.* **2010**, *2* (5), 362–368.

(53) Klein Gebbink, R. J. M.; Jonas, R. T.; Goldsmith, C. R.; Stack, T. D. P. A Periodic Walk: A Series of First-Row Transition Metal Complexes with the Pentadentate Ligand PY5. *Inorg. Chem.* **2002**, *41* (18), 4633–4641.

(54) Blackman, A. G. The coordination chemistry of acyclic pentadentate pentaamine ligands. *Polyhedron* **2019**, *161*, 1–33.

(55) Tolmachev, A. A.; Yurchenko, A. A.; Merculov, A. S.; Semenova, M. G.; Zarudnitskii, E. V.; Ivanov, V. V.; Pinchuk, A. M. Phosphorylation of 1-alkylimidazoles and 1-alkylbenzimidazoles with phosphorus(III) halides in the presence of bases. *Heteroat. Chem.* **1999**, *10* (7), 585–597.

(56) Zadrożny, J. M.; Freedman, D. E.; Jenkins, D. M.; Harris, T. D.; Iavarone, A. T.; Mathonière, C.; Clérac, R.; Long, J. R. Slow Magnetic Relaxation and Charge-Transfer in Cyanato-Bridged Coordination Clusters Incorporating $[\text{Re}(\text{CN})_7]^{3-/-}$. *Inorg. Chem.* **2010**, *49* (19), 8886–8896.

(57) Villeneuve, N. M.; Schroeder, R. R.; Ochrymowycz, L. A.; Rorabacher, D. B. Cyclic Voltammetric Evaluation of Rate Constants for Conformational Transitions Accompanying Electron Transfer. Effect of Varying Structural Constraints in Copper(II/I) Complexes with DicyclohexanediyI-Substituted Macrocyclic Tetrathiaethers. *Inorg. Chem.* **1997**, *36* (20), 4475–4483.

(58) Sun, Y.; Bigi, J. P.; Piro, N. A.; Tang, M. L.; Long, J. R.; Chang, C. J. Molecular Cobalt Pentapyridine Catalysts for Generating Hydrogen from Water. *J. Am. Chem. Soc.* **2011**, *133* (24), 9212–9215.

(59) Dudev, T.; Lim, C. Tetrahedral vs Octahedral Zinc Complexes with Ligands of Biological Interest: A DFT/CDM Study. *J. Am. Chem. Soc.* **2000**, *122* (45), 11146–11153.

(60) Derrick, J. S.; Loipersberger, M.; Chatterjee, R.; Iovan, D. A.; Smith, P. T.; Chakarawet, K.; Yano, J.; Long, J. R.; Head-Gordon, M.; Chang, C. J. Metal–Ligand Cooperativity via Exchange Coupling Promotes Iron- Catalyzed Electrochemical CO₂ Reduction at Low Overpotentials. *J. Am. Chem. Soc.* **2020**, *142* (48), 20489–20501.

(61) Deeba, R.; Chardon-Noblat, S.; Costentin, C. Importance of Ligand Exchange in the Modulation of Molecular Catalysis: Mechanism of the Electrochemical Reduction of Nitrous Oxide with Rhenium Bipyridyl Carbonyl Complexes. *ACS Catal.* **2023**, *13*, 8262–8272.

(62) Schröder, J.; Himmel, D.; Kratzert, D.; Radtke, V.; Richert, S.; Weber, S.; Böttcher, T. Isolation of a stable pyridine radical anion. *Chem. Commun.* **2019**, *55* (9), 1322–1325.

(63) Ekanayake, D. M.; Kulesa, K. M.; Singh, J.; Kpogo, K. K.; Mazumder, S.; Bernhard Schlegel, H.; Verani, C. N. A pentadentate nitrogen-rich copper electrocatalyst for water reduction with pH-dependent molecular mechanisms. *Dalton Trans.* **2017**, *46* (48), 16812–16820.